One-Step ^{18}F-Labeling and Preclinical Evaluation of Prostate-Specific Membrane Antigen Trifluoroborate Probes for Cancer Imaging

Hsiou-Ting Kuo*[1,2], Mathieu L. Lepage*[3], Kuo-Shyan Lin[1,2], Jinhe Pan[1], Zhengxing Zhang[1], Zhibo Liu[3], Alla Pryyma[3], Chengcheng Zhang[1], Helen Merkens[1,2], Aron Roxin[1,3], David M. Perrin[3], and François Bénard[1,2]

[1]*BC Cancer, Vancouver, British Columbia, Canada;* [2]*Department of Radiology, University of British Columbia, Vancouver, British Columbia, Canada; and* [3]*Chemistry Department, University of British Columbia, Vancouver, British Columbia, Canada*

After the identification of the high-affinity glutamate-ureido scaffold, the design of several potent ^{18}F- and ^{68}Ga-labeled tracers has allowed spectacular progress in imaging recurrent prostate cancer by targeting the prostate-specific membrane antigen (PSMA). We evaluated a series of PSMA-targeting probes that are ^{18}F-labeled in a single step for PET imaging of prostate cancer. **Methods:** We prepared 8 trifluoroborate constructs for prostate cancer imaging, to study the influence of the linker and the trifluoroborate prosthetic on pharmacokinetics and image quality. After 1-step labeling by ^{19}F–^{18}F isotopic exchange, the radiotracers were injected in mice bearing LNCaP xenografts, with or without blocking controls, to assess specific uptake. PET/CT images and biodistribution data were acquired at 1 h after injection and compared with ^{18}F-DCFPyL on the same mouse strain and tumor model. **Results:** All tracers exhibited nanomolar affinities, were labeled in good radiochemical yields at high molar activities, and exhibited high tumor uptake in LNCaP xenografts with clearance from nontarget organs. Most derivatives with a naphthylalanine linker showed significant gastrointestinal excretion. A radiotracer incorporating this linker with a dual trifluoroborate-glutamate labeling moiety showed high tumor uptake, low background activity, and no liver or gastrointestinal track accumulation. **Conclusion:** PSMA-targeting probes with trifluoroborate prosthetic groups represent promising candidates for prostate cancer imaging because of facile labeling while affording high tumor uptake values and contrast ratios that are similar to those obtained with ^{18}F-DCFPyL.

Key Words: PSMA; ^{18}F-trifluoroborate; ^{18}F labeling; positron emission tomography; prostate cancer

J Nucl Med 2019; 60:1160–1166
DOI: 10.2967/jnumed.118.216598

The prostate-specific membrane antigen (PSMA), a transmembrane metalloenzyme (*1*), is highly overexpressed in prostate cancer and tumor-associated neovasculature (*2*). PSMA-targeting constructs have been designed and evaluated as imaging agents for visualizing prostate cancer, most notably by PET (*3–6*). The diamino acid glutamate-ureido is commonly used for PSMA targeting because of synthetic ease, rapid pharmacokinetics, and high contrast ratios (*7*). ^{68}Ga-PSMA-11 is currently the most commonly used radioligand for prostate cancer imaging (*8,9*). The short half-life of ^{68}Ga (68 min) generally restricts distribution to clinics that are close to a ^{68}Ge–^{68}Ga generator, which itself limits daily production to 2–4 clinical doses unless direct production using a more complex solid-target apparatus is implemented (*10*). In contrast, ^{18}F has several advantages, including a longer half-life (109.8 min); higher spatial resolution than ^{68}Ga due to its short positron range; and on-demand, scalable production of ^{18}F-fluoride ions up to a few hundred gigabecquerels (*11*).

To this effect, ^{18}F-labeled PSMA-targeting radiotracers such as ^{18}F-DCFPyL (*12*) and ^{18}F-PSMA-1007 (*13*) have been introduced in clinical studies. We sought to explore a new ^{19}F–^{18}F isotope exchange reaction on organotrifluoroborate (RBF_3^-) groups to develop PSMA-targeting radiotracers. With this approach, a precursor is converted into a radiotracer of identical chemical composition. Isotope exchange labeling of RBF_3^- groups provides good activity yields (15%–60%) and high molar activity values ($\geq$75 GBq/μmol) (*14,15*). This method has been successfully applied to several ^{18}F-RBF_3^-–based radiotracers (*15–23*).

We report the synthesis, radiolabeling, and PET imaging of radiotracers based on the glutamate-ureido-lysine scaffold bearing RBF_3^- radioprosthetic groups (compounds **1–8**, Fig. 1). We measured their binding affinity toward PSMA and $LogD_{7.4}$ values and then acquired PET images and ex vivo biodistribution data in mice bearing PSMA-expressing LNCaP prostate cancer xenografts. These results were compared with those of ^{18}F-DCFPyL, a clinically emergent ^{18}F-labeled tracer for prostate cancer imaging.

Received Jun. 26, 2018; revision accepted Jan. 13, 2019.
For correspondence or reprints contact the following: Francois Benard, BC Cancer Research Centre, 675 West 10th Ave., Vancouver, BC, V5Z 1L3, Canada.
E-mail: fbenard@bccrc.ca
David Perrin, Chemistry Department, 2036 Main Mall, University of British Columbia, Vancouver, BC, V6T 1Z1, Canada.
E-mail: dperrin@chem.ubc.ca
Kuo-Shyan Lin, BC Cancer Research Centre, 675 West 10th Ave., Vancouver, BC, V5Z 1L3, Canada.
E-mail: klin@bccrc.ca
*Contributed equally to this work.
Published online Feb. 8, 2019.

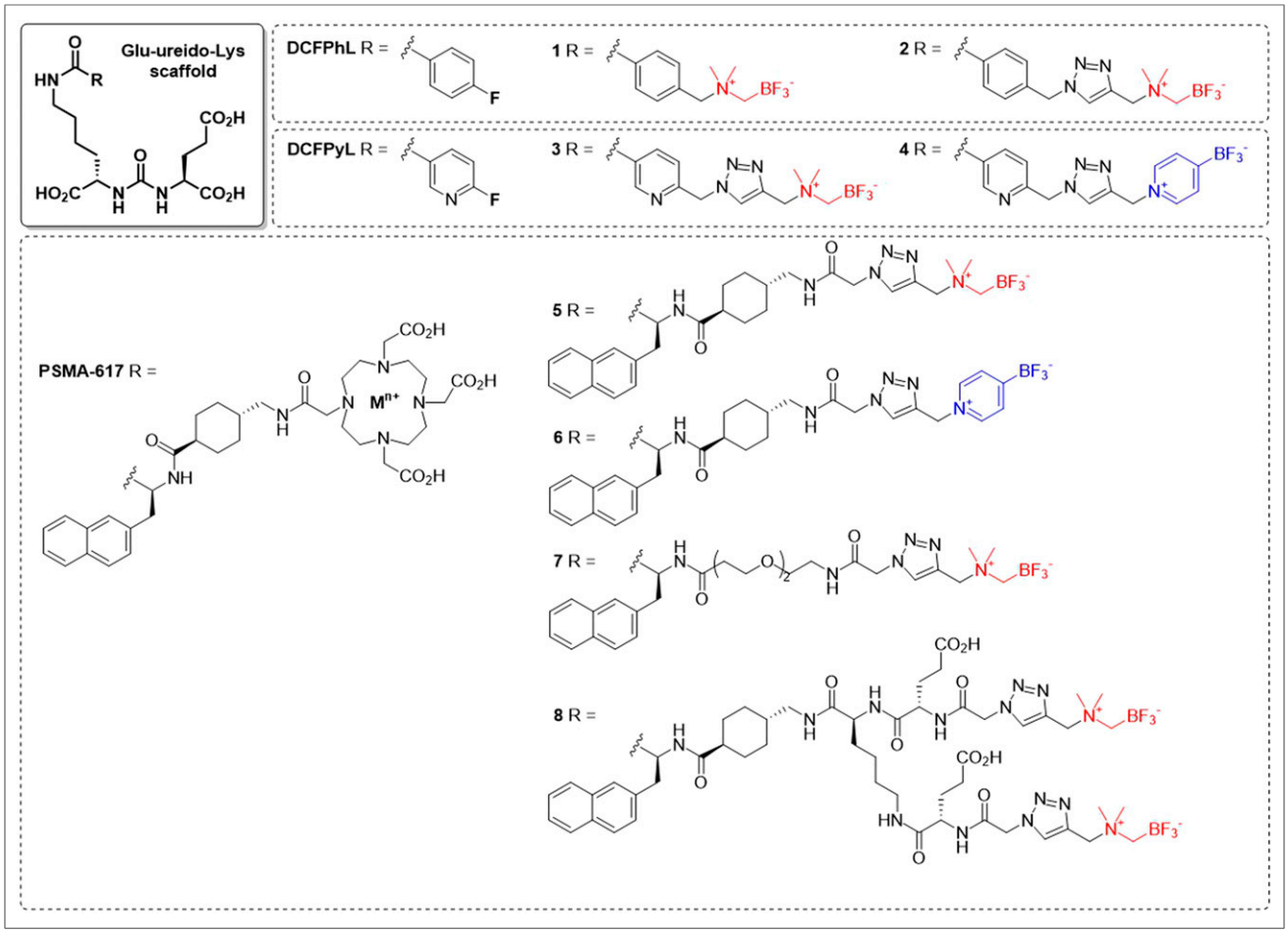

FIGURE 1. Trifluoroborate probes resembling scaffolds of DCFPhL, DCFPyL, and PSMA-617. In red: $AMBF_3$ prosthetic; in blue: $pyrBF_3$ prosthetic.

MATERIALS AND METHODS

Synthesis of Trifluoroborate Probes and Radiosynthesis

^{18}F-DCFPyL was prepared following literature procedures (*24*). Precursors for tracers **1–8** were synthesized as described in the supplemental data section (available at http://jnm.snmjournals.org) to give azide-bearing precursors (*6*,*18*,*21*,*24–28*), which were conjugated to previously reported alkyne-bearing RBF_3^- (*19*). After conjugation, the final trifluoroborate conjugate was purified by high-performance liquid chromatography (HPLC), and purity was confirmed by electrospray ionization–mass spectrometry. Representative crude and quality control HPLC traces are provided in the supplemental data section. ^{18}F-**1–8** were labeled via previously reported procedures (*15*,*29*). Briefly, 30–40 GBq of no-carrier-added ^{18}F-fluoride were trapped on a QMA light cartridge and eluted with 0.9% saline or phosphate-buffered saline (typically 100 μL) directly into a septum-sealed falcon tube containing 80–100 nmol of precursors **1–8** dissolved in 50:50 dimethylformamide:water containing 1 M pyridazinium-HCl buffer (pH 2.5). The reaction was heated to 80°C, and a vacuum was applied to reduce the reaction volume. After 15–20 min, the reaction was quenched by addition of 2 mL of 40 mM ammonium formate or phosphate-buffered saline, and the contents were purified by semipreparative HPLC. Radiochemical purity was confirmed by HPLC analysis using an analytic RP-C18 column with gradients of acetonitrile and water (both containing 0.1% trifluoroacetic acid). Measurements of molar activity values were based on standard curve analysis.

Cell Culture

The LNCaP cell line was obtained from ATCC (LNCaP clone FGC, CRL-1740). The cells were cultured in RPMI 1640 medium supplemented with 10% fetal bovine serum, penicillin (100 U/mL), and streptomycin (100 μg/mL) at 37°C in a MCO-19AIC (Panasonic Healthcare) humidified incubator containing 5% CO_2. Cells grown to 80%–90% confluence were then washed with sterile phosphate-buffered saline (1 × phosphate-buffered saline, pH 7.4) and trypsinized. The collected cell number was counted with a Bal Supply 202C laboratory counter.

In Vitro Competition Binding Assay

Inhibition constants (K_i) of **1–8** and DCFPyL to PSMA were measured by in vitro competition binding assays using ^{18}F-DCFPyL as the radioligand. LNCaP cells were plated onto a 24-well poly-D-lysine coated plate for 48 h (400,000/well). Growth medium was removed and replaced with 4-(2-hydroxyethyl)-1-piperazineethanesulfonic acid (HEPES) buffered saline (50 mM HEPES, pH 7.5, 0.9% sodium chloride) After 1 h, ^{18}F-DCFPyL (0.1 nM) was added to each well (in triplicate) containing varied concentrations (0.5 mM–0.05 nM) of tested compounds (DCFPyL, **1–8**). Nonspecific binding was determined in the presence of 10 μM unlabeled DCFPyL. The assay mixtures were incubated for 1 h at 37°C with gentle agitation followed by 2 washes with cold HEPES buffered saline. A trypsin solution (0.25%, 400 μL) was then added to each well to harvest the cells.

TABLE 1
Activity Yield, Molar Activity, Partition Coefficient, and Binding Affinity of ^{18}F-Labeled PSMA Radiotracers

Tracer	Activity yield* (%, isolated)	Molar activity† (GBq/μmol)	$LogD_{7.4}$ (n = 3)	K_i (nM) (n = 3)
^{18}F-DCFPyL	12 ± 3 (n = 7)	118 ± 37 (n = 7)	−3.12 ± 0.22	2.0 ± 0.8
^{18}F-**1**	7 ± 4 (n = 4)	70 ± 19 (n = 4)	−3.43 ± 0.35	14.4 ± 2.7
^{18}F-**2**	4 ± 2 (n = 3)	89 ± 26 (n = 3)	−4.26 ± 0.04	11.8 ± 0.9
^{18}F-**3**	5 ± 1 (n = 3)	56 ± 15 (n = 3)	−4.01 ± 0.14	25.9 ± 5.7
^{18}F-**4**	16 ± 2 (n = 3)	148 ± 89 (n = 3)	−3.34 ± 0.02	27.6 ± 3.8
^{18}F-**5**	13 ± 10 (n = 2)	137 ± 22 (n = 2)	−3.52 ± 0.21	1.14 ± 0.26
^{18}F-**6**	15 ± 2 (n = 6)	278 ± 73 (n = 6)	−2.28 ± 0.01	1.90 ± 0.68
^{18}F-**7**	10 ± 5 (n = 3)	92 ± 22 (n = 2)	−3.24 ± 0.03	16.5 ± 5.5
^{18}F-**8**	7 ± 6 (n = 3)	211 ± 48 (n = 3)	−3.58 ± 0.36	0.22 ± 0.01

*Activity yields are reported at end of synthesis (1 h for DCFPyL, 40 min for **1**–**8**) (with no correction for decay).
†Molar activities are reported at time of quality control injection, shortly after end of synthesis.

Radioactivity was measured by γ-counting, and K_i values were calculated using the "1 site—fit K_i" built-in model in Prism 7 (GraphPad). The dissociation constant value for ^{18}F-DCFPyL, used for K_i determination, was 0.49 nM, as previously measured by saturation assays using LNCaP cells (*30*).

Distribution Coefficient ($LogD_{7.4}$) Measurements

$LogD_{7.4}$ values were measured using the shake flask method. Briefly, an aliquot of ^{18}F-labeled tracer was added to a vial containing 2.5 mL of *n*-octanol and 2.5 mL of phosphate buffer (0.1 M, pH 7.4). The mixture was vortexed for 2 min and then centrifuged at 3,000*g* for 10 min. A sample of the *n*-octanol (0.1 mL) and buffer (0.1 mL) layers was counted using a γ-counter. Values of $LogD_{7.4}$ were calculated using the following equation: $LogD_{7.4} = \log_{10}$ [(counts in *n*-octanol phase)/(counts in buffer phase)].

PET/CT Imaging and Biodistribution Studies

Imaging and biodistribution experiments were performed using NODSCID IL2RγKO male mice. All experiments were conducted according to the guidelines established by the Canadian Council on Animal Care and approved by the Animal Ethics Committee of the University of British Columbia. Mice were anesthetized by inhalation with 2% isoflurane in oxygen and implanted subcutaneously with 1×10^7 LNCaP cells behind the left shoulder. The mice were imaged or used in biodistribution studies once the tumor reached 5–8 mm in diameter (5–6 wk).

PET imaging experiments were conducted using an Inveon preclinical PET/CT scanner (Siemens). Compounds ^{18}F-**1,2,3,5,7,** and **8** were formulated in 10% ethanol/normal saline, whereas ^{18}F-**4** and **6** were formulated in 10% ethanol/phosphate-buffered saline. Each tumor-bearing mouse was injected with 6–8 MBq of ^{18}F-**1–8** or ^{18}F-DCFPyL through the tail vein under sedation (2% isoflurane in oxygen). For blocking controls, the mice were coinjected with DCFPyL (0.5 mg). After injection, the mice were allowed to recover and roam freely in their cage. After 50 min, the mice were sedated by 2% isoflurane inhalation and positioned in the scanner. A CT scan was performed first for localization and attenuation correction. This was followed by a 10-min static PET scan. The mice were kept warm by a heating pad during image acquisition. PET images were reconstructed using the IAW software (Siemens), using 2 iterations of the ordered-subset expectation maximization algorithm followed by 18 iterations of the maximum a posteriori algorithm.

For biodistribution and blocking studies, the mice were injected with 1–3 MBq of radiotracer. At 60 min, the mice were anesthetized with 2% isoflurane inhalation and euthanized by CO_2 inhalation. Blood was withdrawn by cardiac puncture, and the organs and tissues of interest were collected, weighed, and counted using an automatic γ-counter (PerkinElmer). Uptake values were expressed as the percentage of the injected dose per gram of tissue (%ID/g).

Statistical Analysis

A standard 1-way ANOVA was performed to determine whether statistically significant differences in tumor uptake occurred between radiotracers. Each radiotracer was compared with ^{18}F-DCFPyL using the Dunnett test (a many-to-one *t* test comparison). This analysis was also performed for kidney and blood activity and for tumor-to-blood and tumor-to-muscle ratios. Reported *P* values were adjusted for multiple comparisons. The analysis was performed using Prism 8 (GraphPad).

RESULTS

Radiolabeling

Starting with 37 GBq of ^{18}F-fluoride, **1**–**8** (80–100 nmol) were successfully labeled within 25 min, with activity yields ranging from 4% to 16% (Table 1) at high molar activities (≥56 GBq/μmol). In all cases, the radiochemical purity was at least 99% by analytic HPLC. Compounds bearing the pyridine-trifluoroborate ($pyrBF_3$) prosthetic (**4, 6**) were labeled in higher yields and molar activities than conjugates bearing the ammoniomethyl-trifluoroborate ($AMBF_3$) prosthetic (**3, 5**). Although HPLC was used to isolate tracers at greater than or equal to 99% radiochemical purity, HPLC purification can be avoided: ^{18}F-**6** was purified on a Sep-Pak C_{18} cartridge according to reported procedures (*29*). In that case, the radiochemical purity was at least 95%. In addition, we deliberately labeled **2** at lower molar activity; starting with 37 GBq of no-carrier-added

TABLE 2
Changes in Activity Yield and Molar Activity with Higher Quantities of Precursor Material

Tracer	Activity yield (%)	Molar activity (GBq/μmol)
^{18}F-**2** from 100 nmol (n = 3)	4 ± 2	89 ± 26
^{18}F-**2** from 1000 nmol (n = 2)	34 ± 9	13.3 ± 0.74
Change	× 8.5	÷ 6.7

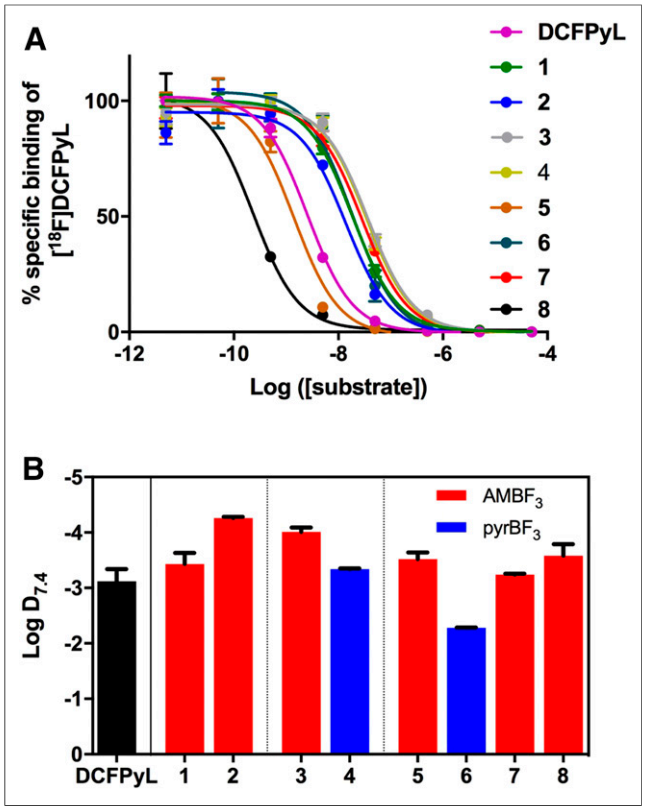

FIGURE 2. (A) Competitive inhibition curves of DCFPyL and **1**–**8**. (B) Values of $LogD_{7.4}$ for DCFPyL and **1**–**8** (error bars reflect SD).

^{18}F-fluoride and 1 μmol of precursor; ^{18}F-**2** was obtained in 34% activity yield at 13.3 GBq/μmol (Table 2).

Binding Assays

We determined K_i via in vitro competition binding assays using LNCaP cells and ^{18}F-DCFPyL as the radioligand (Fig. 2A). The K_i value for DCFPyL was 2.0 ± 0.8 nM, consistent with the value previously reported by Chen et al. (1.1 ± 0.1 nM) (*31*). Probes **1**–**4** and **7** had K_i values in the 10–30 nM range, whereas **5** and **6** had up to 10-fold better affinities, comparable to that measured for DCFPyL. Probe **8** showed excellent binding affinity to PSMA, with a K_i value of 0.22 ± 0.01 nM (Table 1).

$LogD_{7.4}$

All compounds but **6** had $LogD_{7.4}$ values similar to ^{18}F-DCFPyL (Figure 2B and Table 1). Using $pyrBF_3$ instead of $AMBF_3$ as the prosthetic group decreased hydrophilicity in **4** and **6** compared with **3** and **5**, respectively. Compound **6** was the most lipophilic compound of the series.

PET/CT Imaging and Biodistribution

Imaging ^{18}F-DCFPyL confirmed good tumor uptake and fast clearance (*31*). Similarly, ^{18}F-**1**–**8** showed significant tumor uptake in LNCaP xenografts, which was blocked by coinjection of unlabeled DCFPyL (Fig. 3), thus confirming the specificity of tumor uptake for PSMA. All images also showed high, specific kidney uptake along with urinary excretion. Bone accumulation was negligible for all radiotracers. The blocking agent caused significantly lower tumor and kidney uptake values for all compounds.

The tracers based on a naphthylalanine-tranexamic acid linker (**5** and **6**) displayed tumor uptake values of 13.7 ± 5.2 %ID/g and 11.9 ± 2.3 %ID/g, respectively. ^{18}F-**1, 2, 3, 4,** and **7** had uptake values of 6.0 ± 1.2, 8.3 ± 1.3, 4.4 ± 0.95, 6.3 ± 0.8, and 5.1 ± 1.1 %ID/g, respectively. Compounds ^{18}F-**1, 3, 4,** and **7** had lower tumor uptake than ^{18}F-DCFPyL (Fig. 4A). Compound **8** had high tumor uptake (16.7 ± 2.7 %ID/g). No statistically significant differences were observed between compounds **2, 5,** and **6** and ^{18}F-DCFPyL, whereas compound **8** had higher uptake. Compounds **3** and **7** had lower kidney accumulation (Fig. 4B), whereas compounds **5** and **6** had significantly higher intestinal activity than ^{18}F-DCFPyL (Fig. 4C). The blocking controls showed that intestinal uptake was not receptor-mediated. The tumor-to-blood and tumor-to-muscle ratios were not statistically different from ^{18}F-DCFPyL for any compound except compound **7,** which had higher ratios (Fig. 5). Compound **8,** with 2 $AMBF_3$-glutamate motifs, had no significant accumulation in the liver, no hepatobiliary excretion, and low background activity (Fig. 6).

DISCUSSION

We designed PSMA-targeting radiotracers that combine the advantages of 1-step aqueous ^{18}F-labeling afforded by 2 RBF_3^- radioprosthetic groups with certain chemical features found in DCFPyL (or its *C*-analog DCFPhL) (*4*) and PSMA-617 (*32*). Since the 3 carboxylates of Glu-ureido-Lys are needed for binding to PSMA, we introduced modifications at the lysine side chain (*31,33*), off of which we introduced several well-established linkers along with a suitable RBF_3^-.

Binding assays confirmed low-nanomolar affinities for compounds **5** and **6,** whereas compound **8** had subnanomolar binding affinity. Compounds **1**–**4** exhibited 10-fold higher affinities than DCFPyL, suggesting that the trifluoroborate prosthetic group may not interact well with the S1 binding pocket in PSMA, which exhibits pronounced affinity for hydrophobic groups (*3*). Compounds incorporating a naphthylalanine-tranexamic acid motif (**5** and **6**) exhibited improved binding affinities (K_i = 1.14 nM and 1.90 nM,

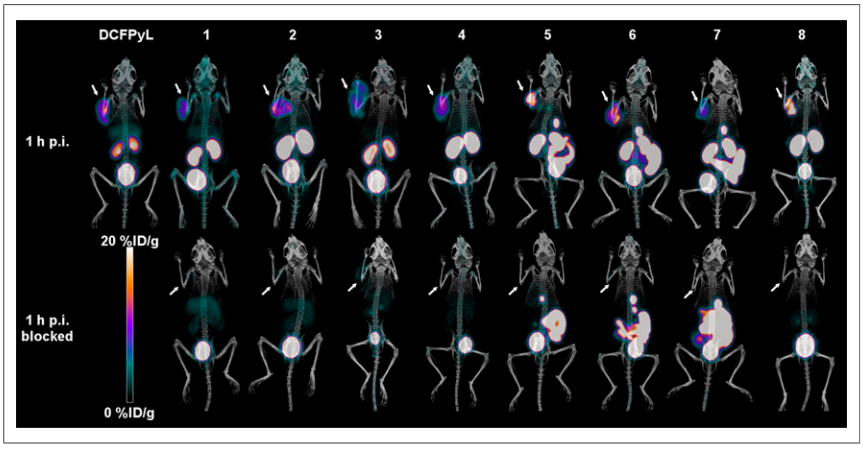

FIGURE 3. PET/CT images (maximum-intensity projections) of LNCaP tumor–bearing mice at 1 h after injection, with and without blocking by coinjection of unlabeled DCFPyL. Arrows locate tumors.

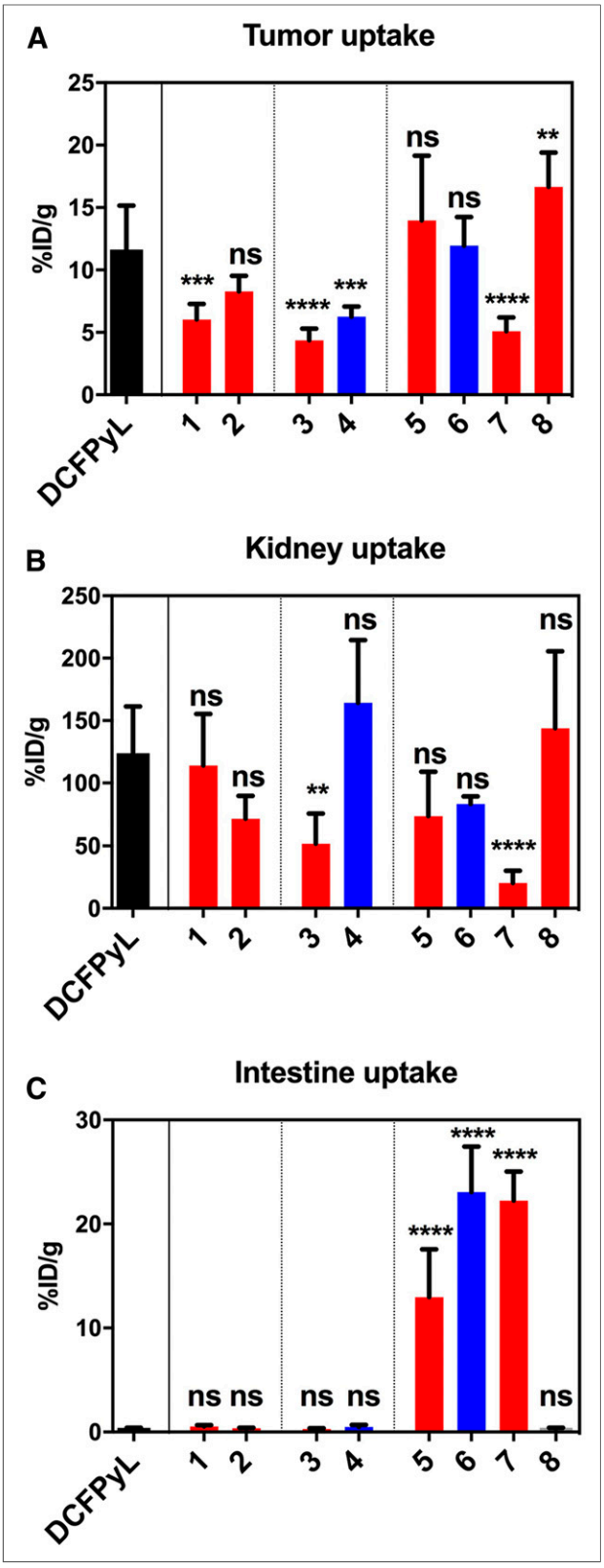

FIGURE 4. Uptake values for tumor (A), kidney (B), and intestine (C) for compounds **1**–**8** and DCFPyL; in black: DCFPyL; in red: $AMBF_3$ derivatives; in blue: $pyrBF_3$ derivatives (error bars reflect SD values, significance of differences with ^{18}F-DCFPyL indicated at top of bars: $^{**}P < 0.01$; $^{****}P < 0.0001$; ns = not significant). Full data available in Supplemental Data section.

respectively) similar to those of DCFPyL (K_i = 2.0 nM) and Ga-PSMA-617 (K_i = 2.3 nM) (*25*). Interestingly, the tranexamic acid linker appears to contribute significantly to affinity, as its replacement by a polyethylene glycol 2 spacer (compound **7**) resulted in a higher K_i. The dual glutamate-BF_3 motif, introduced to improve the hydrophilicity of the BF_3 derivatives with a naphthylalanine-tranexamic acid linker, unexpectedly improved the binding affinity of compound **8,** with a K_i approximately an order of magnitude better than DCFPyL.

All the RBF_3^--bioconjugates were radiolabeled at activity yields greater than 1.85 GBq at molar activity values of at least 56 GBq/μmol. The $pyrBF_3$-modified conjugates showed higher activity yields than those modified with the $AMBF_3$, along with higher molar activities, consistent with a report that compared

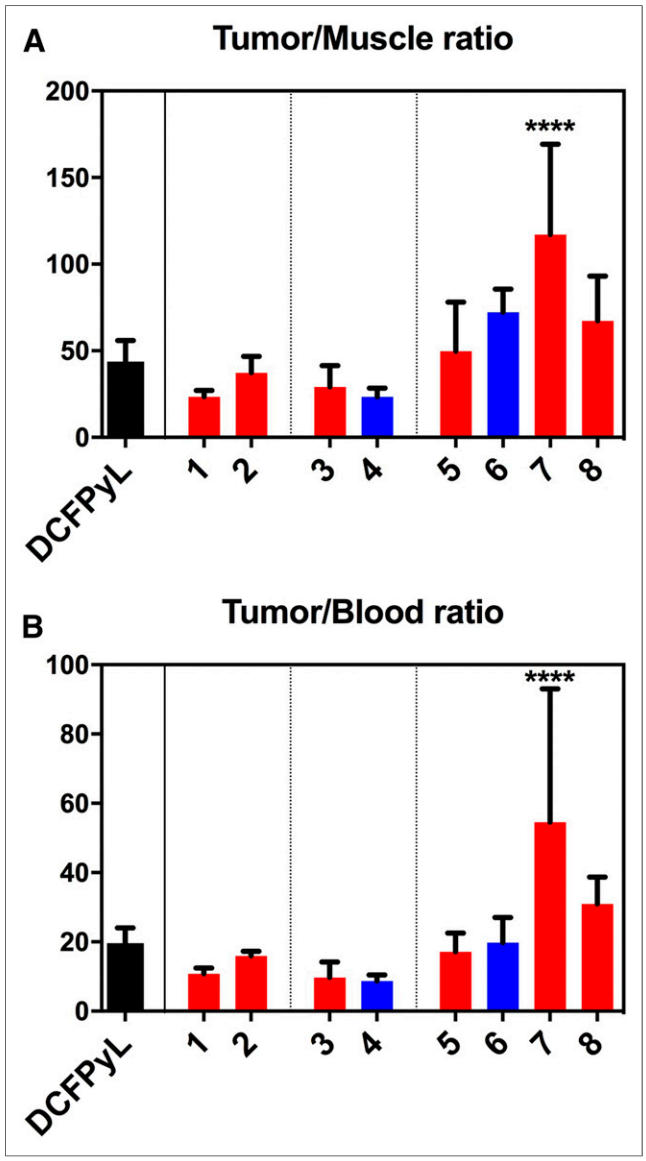

FIGURE 5. Contrast ratios (tumor-to-muscle in A and tumor-to-blood in B) for compounds **1**–**8** and DCFPyL at 1 h after injection; in black: DCFPyL; in red: $AMBF_3$ derivatives; in blue: $pyrBF_3$ derivatives (error bars reflect SD values, significance of differences with ^{18}F-DCFPyL indicated at top of bars: $^{****}P < 0.0001$).

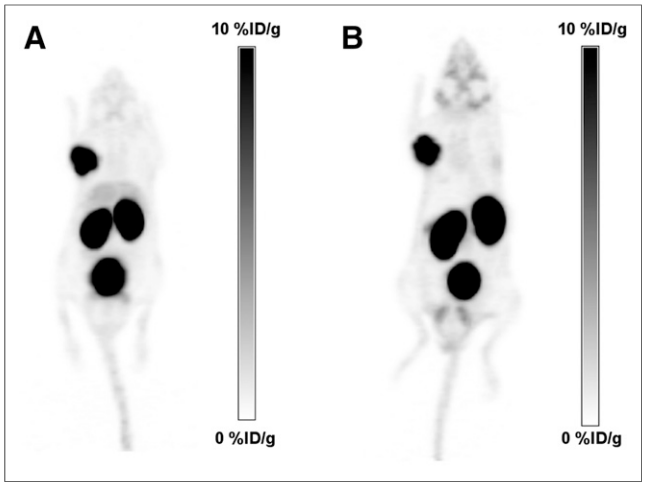

FIGURE 6. PET/CT images (maximum-intensity projections in black on white to display background activity), comparing ^{18}F-DCFPyL (A) with ^{18}F-**8** (B), showing similar image contrast with lower liver accumulation for compound **8**. Maximum of scale corresponds to 10 %ID/g for both radiotracers.

both prosthetic groups in the context of LLP2A-RBF_3^- bioconjugates (*19*), as well as with the established stabilities of various trifluoroborates, as previously reviewed (*34*). High molar activities were also achieved with compound **8,** with a dual glutamate-BF_3 motif. Although imaging and biodistribution studies were performed with HPLC-purified tracers to ensure the highest level of purity, a simple Sep-Pak purification of ^{18}F-**6** (<5 min) afforded good radiochemical purity (95%) (supplemental data). This demonstrates potential for HPLC-free labeling where speed is preferred (overall synthesis time < 30 min).

Although radiochemical yields were lower for certain compounds, these syntheses have not been optimized. Notably, yields were dramatically improved by increasing the amount of precursor: the lowest yield (for tracer ^{18}F-**2**) was increased more than 8-fold to 34% when using 10 times more precursor. Consequently, the average molar activity of ^{18}F-**2** decreased by a similar factor from 89 to 13.3 GBq/μmol. This demonstrates that yields dramatically increase when high molar activity is not critically needed.

To evaluate ^{18}F-**1**–**8** for PSMA imaging, PET/CT imaging and biodistribution studies were conducted in mice bearing LNCaP tumor xenografts. Previously, Chen et al. and Harada et al. imaged ^{18}F-DCFPyL in different strains of mice bearing different tumor models (*31,33*), thus complicating a comparison between this work and prior work. Given these discrepancies, we directly compared ^{18}F-**1**–**8** with ^{18}F-DCFPyL using a single mouse strain and the LNCaP xenograft tumor model, because it expresses PSMA endogenously and is commonly used to evaluate PSMA-targeting radiotracers (*25,33*).

Imaging and biodistribution studies showed that ^{18}F-**1**–**8** and ^{18}F-DCFPyL were all retained in tumors and cleared from nontarget tissues and organs, mainly through the renal pathway for compounds ^{18}F-**1**–**4** and **8,** and a combination of renal and hepatobiliary clearance for compounds ^{18}F-**5**–**7** (Fig. 4). Tumor uptake was higher with ^{18}F-**8** than with ^{18}F-DCFPyL, a result that might be explained by improved affinity. All compounds showed significant renal uptake, which was blocked by DCFPyL, consistent with the well-documented, high PSMA expression in mouse kidneys (*25,31,33,35–38*). As with ^{18}F-DCFPyL, images acquired with ^{18}F-**1**–**4** and **8** showed low uptake in nontarget organs, whereas those acquired with ^{18}F-**5**–**7** showed high accumulation in the gallbladder and intestines. Blocking controls showed that this intestinal uptake was not receptor-mediated. Although it is likely that intestinal uptake is due to the hydrophobic naphthylalanine moiety, this was not noted with ^{68}Ga- or ^{177}Lu-labeled PSMA-617 tracers (*32*). We presume that the DOTA chelator promotes renal clearance.

Because many radiotracers were compared with ^{18}F-DCFPyL, this study did not have statistical power to evaluate small differences between radiotracers. The results confirmed the versatility of RBF_3^- prosthetic groups for ^{18}F radiolabeling, and potential strategies to direct radiotracers to favor hepatobiliary or renal clearance.

Renal clearance can be a drawback for prostate cancer imaging, as focal retention in the ureters may be confused with small nodal metastases, and because high bladder activity may obscure the detection of primary prostate tumors or recurrences. Conversely, excessive bowel activity may also be detrimental for detection of small lesions in the pelvis and abdomen. High liver activity, as observed in clinical studies with ^{18}F-DCFPyL (*12*) and ^{18}F-PSMA-1007 (*13*), might impair detection of liver tumors, notably for detection of hepatocellular carcinomas, for which PSMA imaging may be of value (*39*).

Other ^{18}F-labeled PSMA binding radiotracers have recently been reported, notably ^{18}F-PSMA-1007 (*13,40*), among others (*41–44*). The RBF_3^- radiotracers presented in this article were not directly compared with these compounds. With an excellent binding affinity, high tumor accumulation, and no liver or gastrointestinal excretion, ^{18}F-**8** represents an attractive radiopharmaceutical for clinical translation.

CONCLUSION

We report promising alternatives to current ^{18}F- and ^{68}Ga-labeled PSMA-targeting agents, as the RBF_3^- prosthetic groups enable a facile, 1-step ^{18}F-labeling in aqueous medium. Labeling times could be further reduced to 30 min with a simple Sep-Pak purification. The 1-step labeling by isotope exchange provided for the simple production of a precursor that is chemically identical to the radiolabeled product, simplifying aspects of both production and labeling. These radiotracers were designed to explore the influence of both the spacer and the trifluoroborate prosthetic group. Compound **8,** with a naphthylalanine-tranexamic acid linker and a dual glutamate-BF_3 moiety designed to enhance hydrophilicity, showed excellent binding affinity and high tumor uptake without liver accumulation or hepatobiliary clearance.

DISCLOSURE

This work depicts compounds pertaining to patent WO 2017/117687 A1, which entitles certain authors (Hsiou-Ting Kuo, Mathieu Lepage, Jinhe Pan, Zhibo Liu, Aron Roxin, François Bénard, Kuo-Shyan Lin, and David Perrin) to royalties upon licensing. This work was supported by the Michael Smith Foundation for Health Research, the Canadian Cancer Society (grant #704366), and the Canadian Institutes for Health Research (grant #FDN-148465). No other potential conflict of interest relevant to this article was reported.

ACKNOWLEDGMENTS

We thank Nadine Colpo and Navjit Hundal-Jabal for their help with the animal studies.

REFERENCES

1. Carter RE, Feldman AR, Coyle JT. Prostate-specific membrane antigen is a hydrolase with substrate and pharmacologic characteristics of a neuropeptidase. *Proc Natl Acad Sci USA.* 1996;93:749–753.
2. Silver DA, Pellicer I, Fair WR, Heston WD, Cordon-Cardo C. Prostate-specific membrane antigen expression in normal and malignant human tissues. *Clin Cancer Res.* 1997;3:81–85.
3. Byun Y, Mease RC, Lupold SE, Pomper MG. Recent development of diagnostic and therapeutic agents targeting glutamate carboxypeptidase II (GCPII). In: Supporan CT, Winum J-Y, eds. *Drug Design of Zinc-Enzyme Inhibitors.* Hoboken, NJ: John Wiley & Sons, Inc.; 2009:881–910.
4. Chen Y, Foss CA, Byun Y, et al. Radiohalogenated prostate-specific membrane antigen (PSMA)-based ureas as imaging agents for prostate cancer. *J Med Chem.* 2008;51:7933–7943.
5. Maurer T, Eiber M, Schwaiger M, Gschwend JE. Current use of PSMA-PET in prostate cancer management. *Nat Rev Urol.* 2016;13:226–235.
6. Maresca KP, Hillier SM, Femia FJ, et al. A series of halogenated heterodimeric inhibitors of prostate specific membrane antigen (PSMA) as radiolabeled probes for targeting prostate cancer. *J Med Chem.* 2009;52:347–357.
7. Kiess AP, Banerjee SR, Mease RC, et al. Prostate-specific membrane antigen as a target for cancer imaging and therapy. *Q J Nucl Med Mol Imaging.* 2015;59:241–268.
8. Lütje S, Heskamp S, Cornelissen AS, et al. PSMA ligands for radionuclide imaging and therapy of prostate cancer: clinical status. *Theranostics.* 2015;5: 1388–1401.
9. Calais J, Fendler WP, Herrmann K, Eiber M, Ceci F. Comparison of ^{68}Ga-PSMA-11 and ^{18}F-fluciclovine PET/CT in a case series of 10 patients with prostate cancer recurrence. *J Nucl Med.* 2018;59:789–794.
10. Lin M, Waligorski GJ, Lepera CG. Production of curie quantities of Ga-68 with a medical cyclotron via the Zn-68 (p,n)Ga-68 reaction. *Appl Radiat Isot.* 2018;133:1–3.
11. Eberl S, Eriksson T, Svedberg O, et al. High beam current operation of a PETtrace (TM) cyclotron for F-18(−) production. *Appl Radiat Isot.* 2012;70:922–930.
12. Szabo Z, Mena E, Rowe SP, et al. Initial evaluation of [^{18}F]DCFPyL for prostate-specific membrane antigen (PSMA)-targeted PET imaging of prostate cancer. *Mol Imaging Biol.* 2015;17:565–574.
13. Giesel FL, Hadaschik B, Cardinale J, et al. F-18 labelled PSMA-1007: biodistribution, radiation dosimetry and histopathological validation of tumor lesions in prostate cancer patients. *Eur J Nucl Med Mol Imaging.* 2017;44: 678–688.
14. Liu Z, Li Y, Lozada J, Lin K-S, Schaffer P, Perrin DM. Rapid, one-step, high yielding ^{18}F-labeling of an aryltrifluoroborate bioconjugate by isotope exchange at very high specific activity. *J Labelled Comp Radiopharm.* 2012;14:491–497.
15. Liu Z, Pourghiasian M, Radtke MA, et al. An organotrifluoroborate for broadly applicable one-step F-18-labeling. *Angew Chem Int Ed Engl.* 2014;53:11876–11880.
16. Zhang Z, Jenni S, Zhang CC, et al. Synthesis and evaluation of F-18-trifluoroborate derivatives of triphenylphosphonium for myocardial perfusion imaging. *Bioorg Med Chem Lett.* 2016;26:1675–1679.
17. Lau J, Liu ZB, Lin KS, et al. Trimeric radiofluorinated sulfonamide derivatives to achieve in vivo selectivity for carbonic anhydrase IX-targeted PET imaging. *J Nucl Med.* 2015;56:1434–1440.
18. Liu ZB, Pourghiasian M, Benard F, Pan JH, Lin KS, Perrin DM. Preclinical evaluation of a high-affinity F-18-trifluoroborate octreotate derivative for somatostatin receptor imaging. *J Nucl Med.* 2014;55:1499–1505.
19. Roxin Á, Zhang C, Huh S, et al. Preliminary evaluation of ^{18}F-labeled LLP2A-trifluoroborate conjugates as VLA-4 ($\alpha_4\beta_1$ integrin) specific radiotracers for PET imaging of melanoma. *Nucl Med Biol.* 2018;61:11–20.
20. Zhang C, Zhang Z, Lin K-S, et al. Melanoma imaging using ^{18}F-labeled alpha-melanocyte-stimulating hormone derivatives with positron emission tomography. *Mol Pharm.* 2018;15:2116–2122.
21. Pourghiasian M, Liu ZB, Pan JH, et al. F-18-AmBF3-MJ9: a novel radiofluorinated bombesin derivative for prostate cancer imaging. *Bioorg Med Chem.* 2015;23:1500–1506.
22. Liu Z, Amouroux G, Zhang ZX, et al. F-18-trifluoroborate derivatives of Des-Arg(10) kallidin for imaging bradykinin B1 receptor expression with positron emission tomography. *Mol Pharm.* 2015;12:974–982.
23. Liu Z, Radtke MA, Wong MQ, Lin K-S, Yapp DT, Perrin DM. Dual mode fluorescent ^{18}F-PET tracers: efficient modular synthesis of rhodamine-[cRGD] 2-[^{18}F]-organotrifluoroborate, rapid, and high yielding one-step ^{18}F-labeling at high specific activity, and correlated in vivo PET imaging and ex vivo fluorescence. *Bioconjug Chem.* 2014;25:1951–1962.
24. Bouvet V, Wuest M, Jans H-S, et al. Automated synthesis of [^{18}F]DCFPyL via direct radiofluorination and validation in preclinical prostate cancer models. *EJNMMI Res.* 2016;6:40.
25. Benešová M, Schafer M, Bauder-Wust U, et al. Preclinical evaluation of a tailor-made DOTA-conjugated PSMA inhibitor with optimized linker moiety for imaging and endoradiotherapy of prostate cancer. *J Nucl Med.* 2015;56: 914–920.
26. Horiuchi T, Chiba J, Uoto K, Soga T. Discovery of novel thieno[2,3-d]pyrimidin-4-yl hydrazone-based inhibitors of Cyclin D1-CDK4: synthesis, biological evaluation, and structure-activity relationships. *Bioorg Med Chem Lett.* 2009;19: 305–308.
27. Mukherjee S, van der Donk WA. Mechanistic studies on the substrate-tolerant lanthipeptide synthetase ProcM. *J Am Chem Soc.* 2014;136:10450–10459.
28. Zhou Z, Fahrni CJ. A fluorogenic probe for the copper(I)-catalyzed azide-alkyne ligation reaction: modulation of the fluorescence emission via (3)(n,pi*)-(1)(pi,pi*) inversion. *J Am Chem Soc.* 2004;126:8862–8863.
29. Liu Z, Lin KS, Benard F, et al. One-step F-18 labeling of biomolecules using organotrifluoroborates. *Nat Protoc.* 2015;10:1423–1432.
30. Kuo HT, Pan J, Zhang Z, et al. Effects of linker modification on tumor-to-kidney contrast of ^{68}Ga-labeled PSMA-targeted imaging probes. *Mol Pharm.* 2018;15: 3502–3511.
31. Chen Y, Pullambhatla M, Foss CA, et al. 2-(3-{1-carboxy-5-[(6-[^{18}F]fluoro-pyridine-3-carbonyl)-amino]-pentyl}-ureido)-pentanedioic acid, [^{18}F]DCFPyL, a PSMA-based PET imaging agent for prostate cancer. *Clin Cancer Res.* 2011;17: 7645–7653.
32. Kratochwil C, Giesel FL, Eder M, et al. [^{177}Lu]lutetium-labelled PSMA ligand-induced remission in a patient with metastatic prostate cancer. *Eur J Nucl Med Mol Imaging.* 2015;42:987–988.
33. Harada N, Kimura H, Onoe S, et al. Synthesis and biologic evaluation of novel F-18-labeled probes targeting prostate-specific membrane antigen for PET of prostate cancer. *J Nucl Med.* 2016;57:1978–1984.
34. Perrin DM. F-18-organotrifluoroborates as radioprosthetic groups for PET imaging: from design principles to preclinical applications. *Acc Chem Res.* 2016;49: 1333–1343.
35. Weineisen M, Schottelius M, Simecek J, et al. Ga-68- and Lu-177-labeled PSMA I&T: optimization of a PSMA-targeted theranostic concept and first proof-of-concept human studies. *J Nucl Med.* 2015;56:1169–1176.
36. Gregor PD, Wolchok JD, Turaga V, et al. Induction of autoantibodies to syngeneic prostate-specific membrane antigen by xenogeneic vaccination. *Int J Cancer.* 2005;116:415–421.
37. Schmittgen TD, Zakrajsek BA, Hill RE, et al. Expression pattern of mouse homolog of prostate-specific membrane antigen (FOLHI) in the transgenic adenocarcinoma of the mouse prostate model. *Prostate.* 2003;55:308–316.
38. Yang D, Holt GE, Velders MP, Kwon ED, Kast WM. Murine six-transmembrane epithelial antigen of the prostate, prostate stem cell antigen, and prostate-specific membrane antigen: prostate-specific cell-surface antigens highly expressed in prostate cancer of transgenic adenocarcinoma mouse prostate mice. *Cancer Res.* 2001;61:5857–5860.
39. Kesler M, Levine C, Hershkovitz D, et al. ^{68}Ga-PSMA is a novel PET-CT tracer for imaging of hepatocellular carcinoma: a prospective pilot study. *J Nucl Med.* July 12, 2018 [Epub ahead of print].
40. Cardinale J, Schafer M, Benesova M, et al. Preclinical evaluation of ^{18}F-PSMA-1007, a new prostate-specific membrane antigen ligand for prostate cancer imaging. *J Nucl Med.* 2017;58:425–431.
41. Rowe SP, Gage KL, Faraj SF, et al. ^{18}F-DCFBC PET/CT for PSMA-based detection and characterization of primary prostate cancer. *J Nucl Med.* 2015;56: 1003–1010.
42. Malik N, Baur B, Winter G, Reske SN, Beer AJ, Solbach C. Radiofluorination of PSMA-HBED via Al^{18}F(2+) chelation and biological evaluations in vitro. *Mol Imaging Biol.* 2015;17:777–785.
43. Behr SC, Aggarwal R, Van Brocklin HF, et al. First-in-human phase I study of CTT1057, a novel ^{18}F labeled imaging agent with phosphoramidate core targeting prostate specific membrane antigen in prostate cancer. *J Nucl Med.* November 21, 2018 [Epub ahead of print].
44. Zlatopolskiy BD, Endepols H, Krapf P, et al. Discovery of ^{18}F-JK-PSMA-7, a novel PET-probe for the detection of small PSMA positive lesions. *J Nucl Med.* November 2, 2018 [Epub ahead of print].